

## Supplementary Information

### Stacked vanadium pentoxide-zinc oxide interface for optically-chargeable supercapacitor

Pankaj Singh Chauhan<sup>1</sup>, Sumana Kumar<sup>1</sup>, Anindita Mondal<sup>1</sup>, Pragya Sharma<sup>1</sup>, Mihir N. Parekh<sup>2</sup>,  
Vinod Panwar<sup>1</sup>, Apparao M. Rao<sup>2</sup>, Abha Misra<sup>1\*</sup>

<sup>1</sup> Department of Instrumentation and Applied Physics, Indian Institute of Science, Bangalore, Karnataka 560012, India

<sup>2</sup> Department of Physics and Astronomy, Clemson Nanomaterials Institute, Clemson University, Clemson, SC 29634, USA

\*Corresponding author: abha@iisc.ac.in

## 1 Digital image of the device



Fig. S1 Digital image of the fabricated symmetric supercapacitor using  $V_2O_5/ZnO/FTO$  electrodes.

## 2 Energy-dispersive X-ray spectroscopy (EDS) analysis of $V_2O_5/ZnO/FTO$

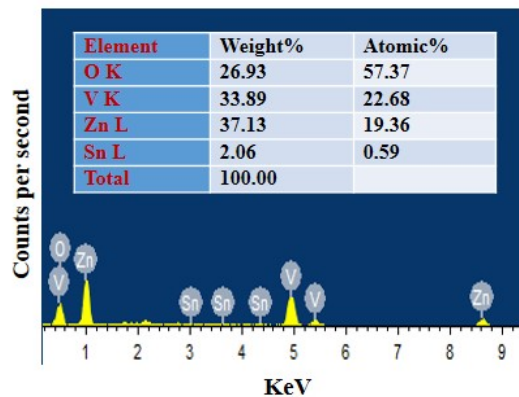
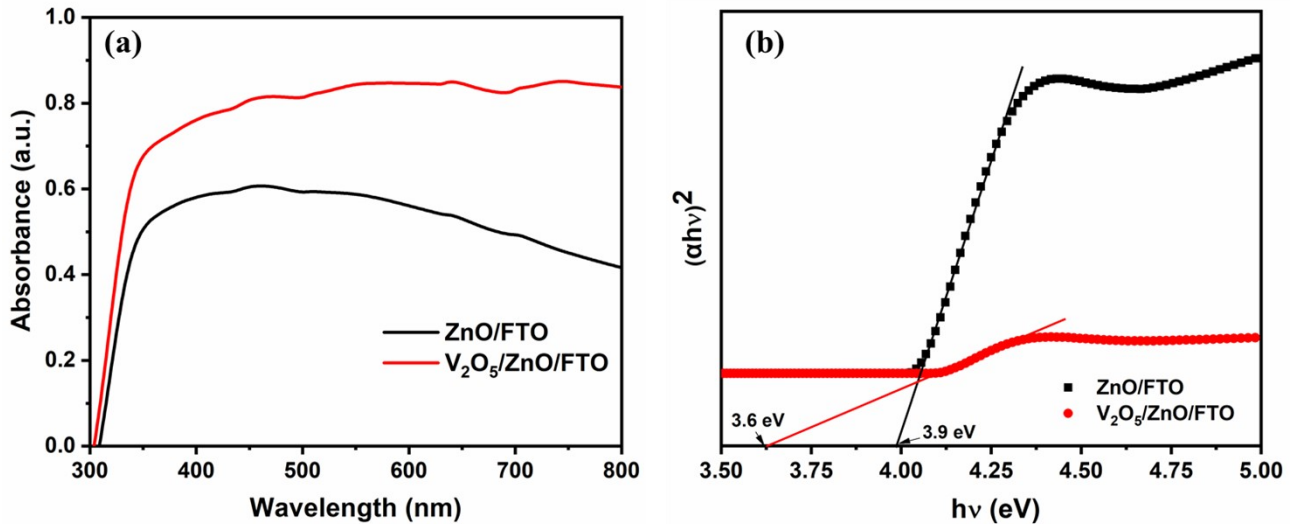


Fig. S2 EDS analysis of the  $V_2O_5/ZnO/FTO$  electrode showing atomic and weight percentages of different elements.

### 3 UV-Visible absorption spectroscopy



*Fig. S3(a)* UV-Visible spectra and (b) corresponding Tauc plots to calculate the band gap of ZnO/FTO and V<sub>2</sub>O<sub>5</sub>/ZnO/FTO heterostructure.

The UV-Visible spectroscopy of the synthesized heterostructure showed good optical absorbance in the UV (315-400 nm) and visible (400-780 nm) range of the electromagnetic spectrum (**Figure S3(a)**).<sup>1</sup> Interestingly, the heterostructured V<sub>2</sub>O<sub>5</sub>/ZnO showed a higher light absorption in the UV and visible range than ZnO, implying that the heterostructure is optically active and suitable for optoelectronic applications. The band gaps were evaluated by plotting  $(\alpha h\nu)^2$  versus photon energy ( $h\nu$ ) (Tauc plots, **Figure S3(b)**) according to Kubelka-Munk theory as:

$$\alpha h\nu = A(h\nu - E_g)^n \quad , \quad (1)$$

where  $\alpha$  is the absorption coefficient of the material,  $A$  is an energy-independent constant,  $h\nu$  is photon energy in eV,  $E_g$  is the material's bandgap, and  $n$  is a constant that depends upon the type of optical transition ( $n = 1/2$ , for direct transition). The calculated band gap values from the Tauc plots are 3.9 eV and 3.6 eV for ZnO/FTO and V<sub>2</sub>O<sub>5</sub>/ZnO/FTO, respectively. The slight reduction

in the bandgap of the heterostructure is advantageous for the electron transfer from the valence band to the conduction band under light irradiation.

#### 4 Raman spectroscopy analysis

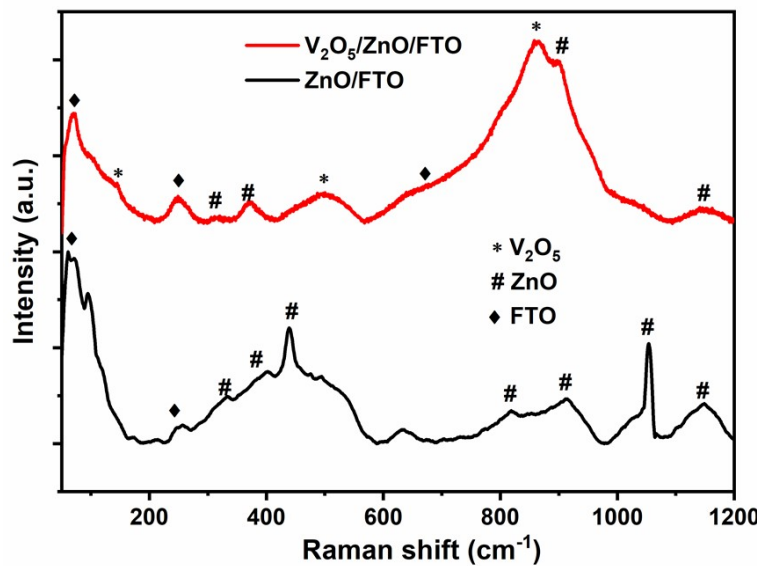


*Fig. S4 Raman spectra of  $\text{ZnO}/\text{FTO}$  and  $\text{V}_2\text{O}_5/\text{ZnO}/\text{FTO}$  heterostructure.*

The Raman spectrum of the synthesized heterostructure is compared to that of  $\text{ZnO}$  in the 50-1200  $\text{cm}^{-1}$  range (**Figure S4**). The peaks at 320, 371, and 437  $\text{cm}^{-1}$  belong to the  $E_2$  mode and the longitudinal mode vibrations of wurtzite  $\text{ZnO}$  nanorods.<sup>2</sup> Similarly, the peak at 1145  $\text{cm}^{-1}$  corresponds to the multi-phonon vibration of  $\text{ZnO}$ .<sup>3</sup> The  $\text{ZnO}$ 's Raman peak at 1055  $\text{cm}^{-1}$  corresponds to the rocking vibration of  $-\text{CH}_3$  from zinc acetate, while peaks at 820 and 916  $\text{cm}^{-1}$  correspond to the C–C stretching vibration of zinc acetate. The peak at 500  $\text{cm}^{-1}$  is due to triply coordinated oxygen ( $\text{V}_3\text{–O}$ ) stretching of the  $\text{V}_2\text{O}_5$  structure.<sup>2</sup> The low-frequency peak at 145  $\text{cm}^{-1}$  shows the layered structure of  $\text{V}_2\text{O}_5$ , which is useful in ion intercalation during electrochemical charge storage. The appearance of a vibrational peak at 850  $\text{cm}^{-1}$  confirms the composite formation

between the two metal oxides.<sup>4</sup> The rest of the peaks correspond to the FTO substrate, some of which are slightly shifted due to the heterostructure formation.

## 5 Fourier transform infrared spectroscopy analysis

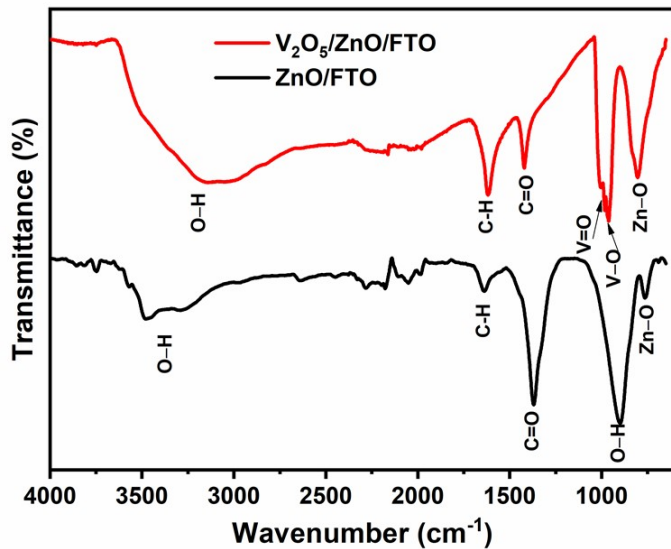


*Fig. S5 FTIR spectra of ZnO/FTO and V<sub>2</sub>O<sub>5</sub>/ZnO/FTO heterostructure.*

The characteristic FTIR transmission spectra of ZnO and V<sub>2</sub>O<sub>5</sub>/ZnO heterostructure are shown in **Figure S5**. The peak at 750 cm<sup>-1</sup> corresponds to the Zn–O stretching mode that confirms the formation of ZnO,<sup>5</sup> while the heterostructure's spectrum shows the 960 and 1000 cm<sup>-1</sup> peaks that correspond to the symmetric stretching vibration of the V–O and V=O bond of vanadyl oxygen, respectively.<sup>6,7</sup> The 1366 cm<sup>-1</sup> peak corresponds to the C=O bond stretching vibration, and the 1622 cm<sup>-1</sup> peak to the C–H vibration resulting from the partial transformation of zinc acetate ions (Zn(CH<sub>3</sub>COO)<sub>2</sub>) into aldehyde during the synthesis.<sup>5,7</sup> The O–H stretching vibration is observed as a broad peak ranging from 3200 to 3600 cm<sup>-1</sup>.

**6      Electrochemical analysis of  $\text{V}_2\text{O}_5/\text{ZnO}/\text{FTO}$  heterostructure in a three-electrode system**

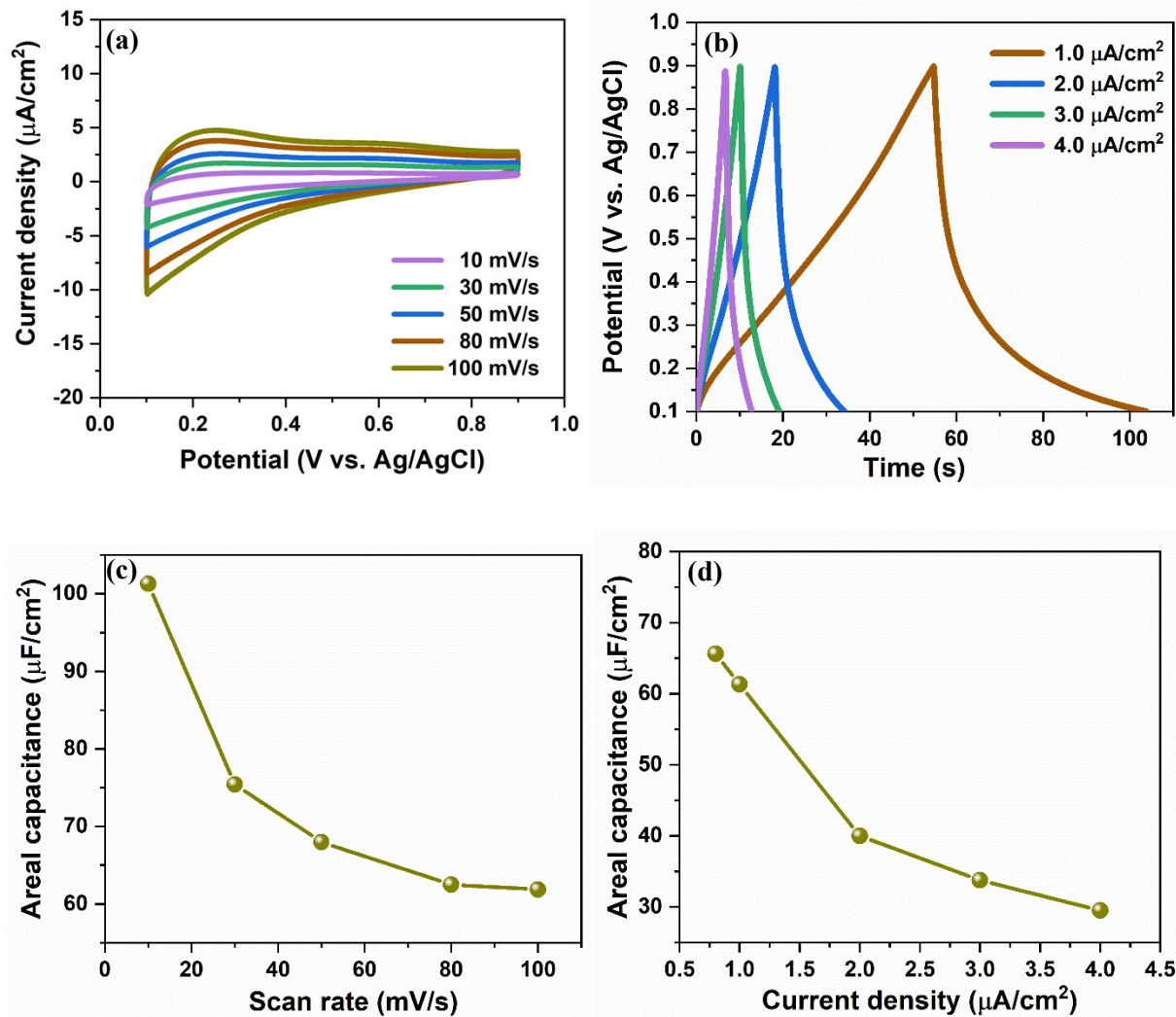


*Fig. S6 (a) CV and (b) GCD curve of  $\text{V}_2\text{O}_5/\text{ZnO}/\text{FTO}$  electrode measured in three-electrode system in the potential range of 0.1 to 0.9 V. (c) and (d) shows corresponding areal capacitance calculated from CV and GCD curve, respectively.*

7 Coulombic efficiency of the  $\text{V}_2\text{O}_5/\text{ZnO}/\text{FTO}$  heterostructure

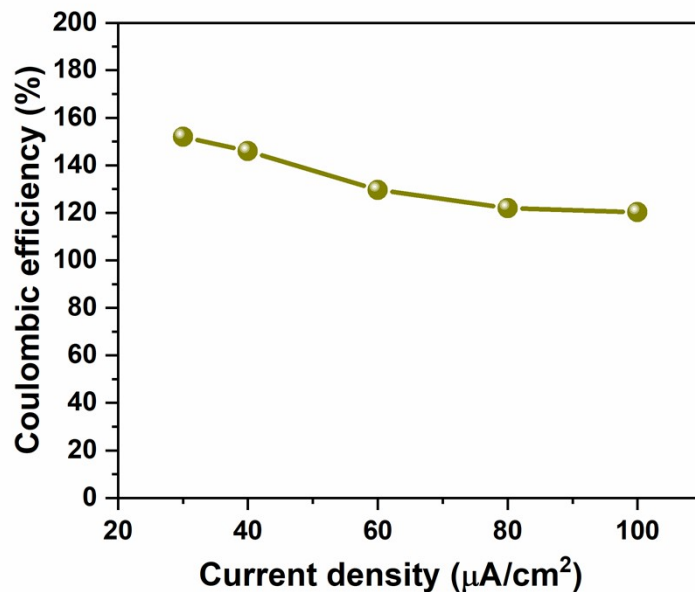


Fig. S7 Coulombic efficiency of  $\text{V}_2\text{O}_5/\text{ZnO}/\text{FTO}$  heterostructure at different current densities.

8 Areal capacitance of device

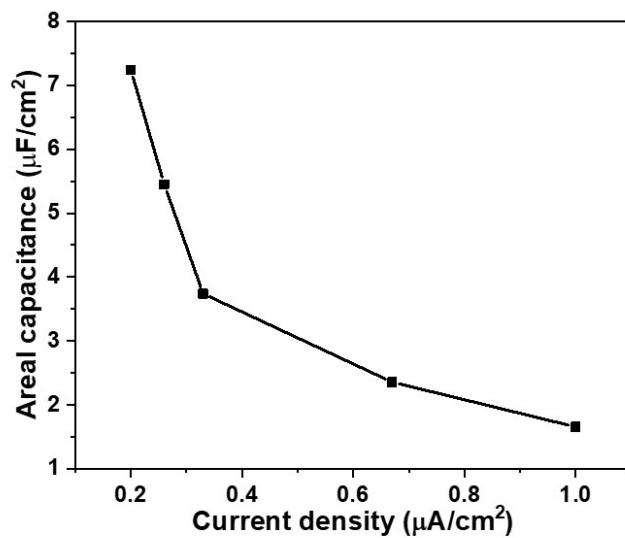
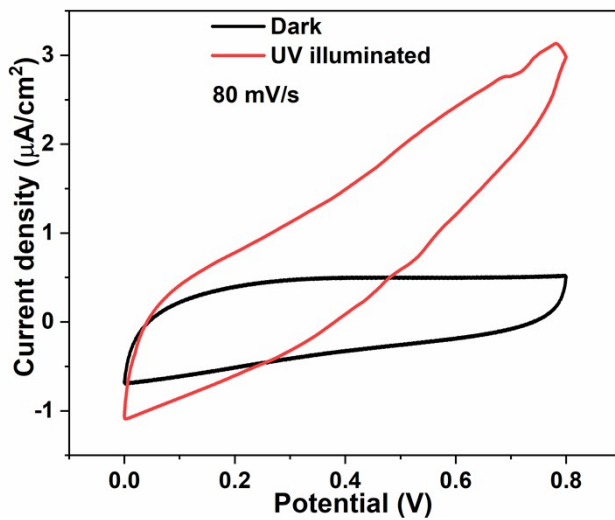


Fig. S8 Areal capacitance ( $C_A$ ) of the device at various current densities calculated from GCD curve using the integration method.

**9 Cyclic voltammetry comparison of the device under dark and UV-illuminated conditions**



*Fig. S9 CV curve of SSD at 80 mV/s scan rate under dark and UV illuminated conditions.*

**10 Capacitance retention**

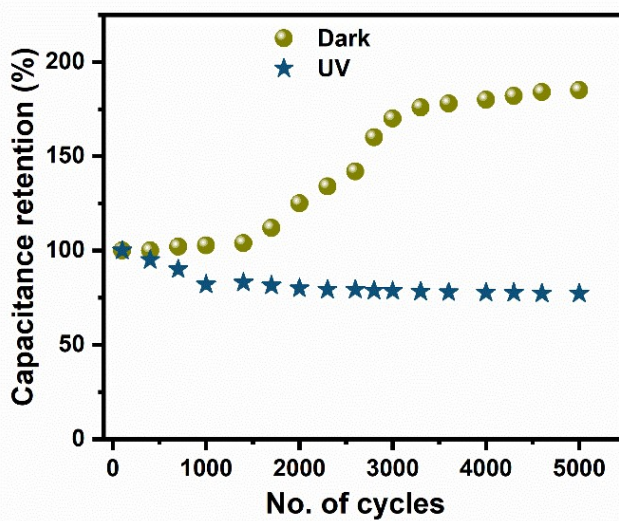


*Fig. S10 Capacitance retention of the supercapacitor under dark and UV illuminated conditions.*

11 Effect of electrochemical cycles on the morphology and structure of  $\text{V}_2\text{O}_5/\text{ZnO}/\text{FTO}$  heterostructure

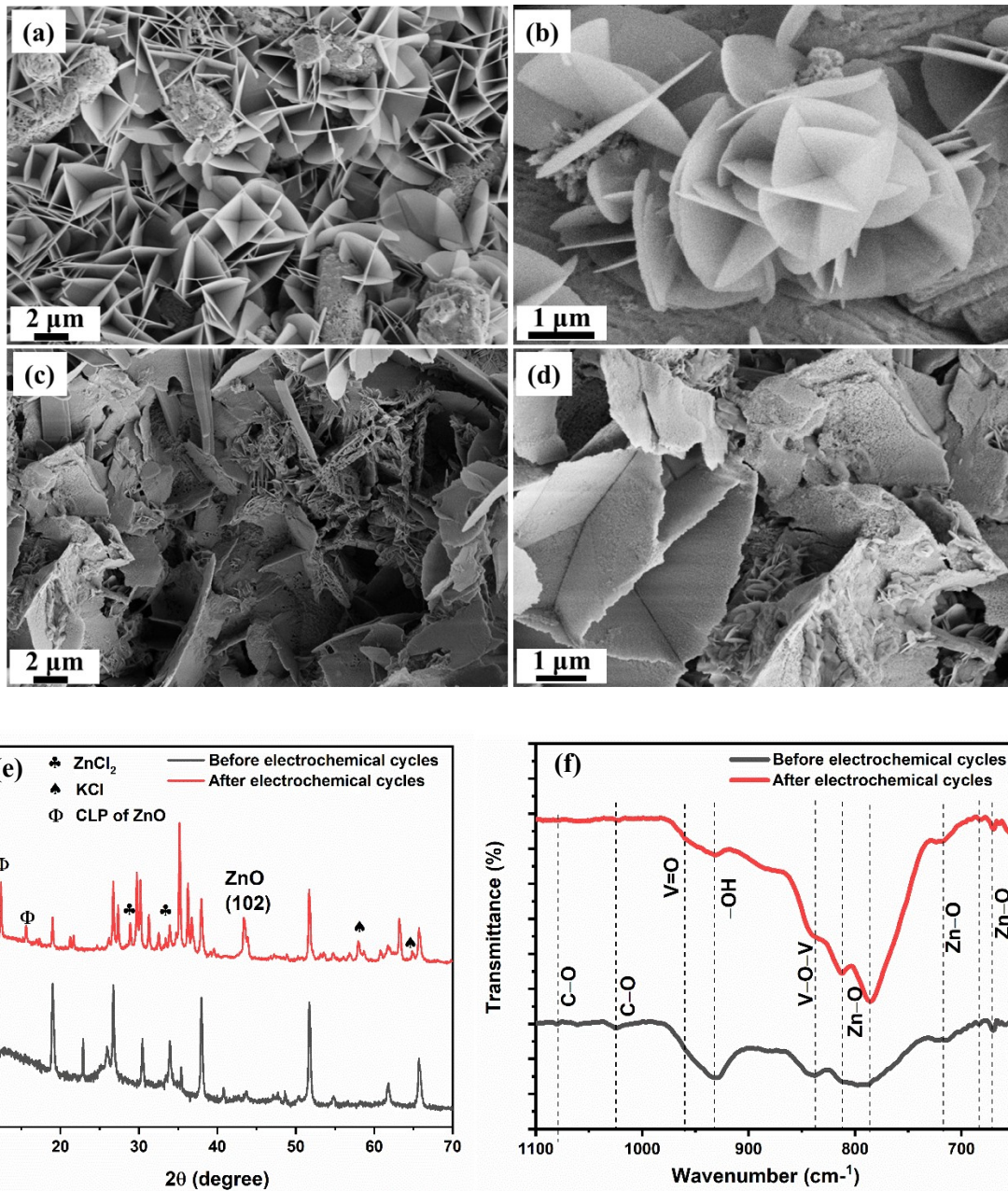


Fig. S11 (a) and (b) SEM images of  $\text{V}_2\text{O}_5/\text{ZnO}/\text{FTO}$  heterostructure before electrochemical cycles. (c) and (d) SEM images of  $\text{V}_2\text{O}_5/\text{ZnO}/\text{FTO}$  heterostructure after 3000 electrochemical cycles. (e) XRD and (f) FTIR analysis of  $\text{V}_2\text{O}_5/\text{ZnO}/\text{FTO}$  heterostructure before and after charge-discharge cycles in 1M KCl electrolyte. (CLP: chloride lamellar phase)

## 12 Comparison with other studies

Table S1: Comparison of V<sub>2</sub>O<sub>5</sub>/ZnO/FTO-based supercapacitor with similar studies conducted in past

S. No.	Material	Electrolyte	Capacitance	Ref.
1	Graphene thin films	PVA/H <sub>3</sub> PO <sub>4</sub>	12.4 µF/cm <sup>2</sup>	14
2	Graphene	PVA/H <sub>2</sub> SO <sub>4</sub>	5.33 µF/cm <sup>2</sup>	15
3	MAPbI <sub>3</sub> perovskite	PVA/KOH/Chlorobenzene	8.06 µF/cm <sup>2</sup>	16
4	graphene-graphene quantum dots chelate	PVA/H <sub>3</sub> PO <sub>4</sub>	9.09 µF/cm <sup>2</sup>	17
5	Silicon nanowires	NEt <sub>4</sub> BF <sub>4</sub> /polycarbonate	6.6 µF/cm <sup>2</sup>	18
6	ZnO nanowires over FTO glass	1M KCl	20 µF/cm <sup>2</sup>	19
7	Multilayer graphene	6M KOH	4 µF/cm <sup>2</sup>	20
8	<b>V<sub>2</sub>O<sub>5</sub>/ZnO/FTO</b>	<b>PVA/KCl</b>	<b>~15 µF/cm<sup>2</sup></b>	<b>This work</b>

## References

- 1 H. Lin, L. Wei, C. Wu, Y. Chen, S. Yan, L. Mei and J. Jiao, *Nanoscale Res. Lett.*, 2016, **11**, 1–7.
- 2 P. S. S. Selvam, G. S. Chinnadurai, D. Ganesan and V. Kandan, *Appl. Phys. A*, 2020, **126**, 1–16.
- 3 R. Zhang, P. Yin, N. Wang and L. Guo, *Solid State Sci.*, 2009, **11**, 865–869.
- 4 P. Nagaraju, Y. Vijayakumar, M. V. Ramana Reddy and U. P. Deshpande, *RSC Adv.*, 2019, **9**, 16515–16524.
- 5 D. D. Thongam, J. Gupta and N. K. Sahu, *SN Appl. Sci.*, 2019, **1**, 1–14.
- 6 J. Aliaga, N. Cifuentes, G. González, C. Sotomayor-Torres and E. Benavente, *Catalysts*, 2018, **8**, 1–13.

- 7 P. Shukla and J. K. Shukla, *J. Sci. Adv. Mater. Devices*, 2018, **3**, 452–455.
- 8 M. Mrad, B. Chouchene and T. Ben Chaabane, *S. Afr. J. Chem.*, 2018, **71**, 103–110.
- 9 M. Li, Y. Liu, W. Han, S. Wang, M. Zhang, Y. Yan and W. Shi, *Metall. Mater. Trans. B*, 2014, **46**.
- 10 X. Lu, G. Li, J. Y. Kim, J. P. Lemmon, V. L. Sprenkle and Z. Yang, *Energy Environ. Sci.*, 2013, **6**, 1837–1843.
- 11 P. S. Chauhan, R. Kant, A. Rai, A. Gupta and S. Bhattacharya, *Mater. Sci. Semicond. Process.*, 2019, **89**, 6–17.
- 12 P. S. Chauhan, K. Kumar, K. Singh and S. Bhattacharya, *Synth. Met.*, 2022, **283**, 116981.
- 13 W. W. Mar and E. Somsook, *ScienceAsia*, 2012, **38**, 90–94.
- 14 Y. Gao, Y. S. Zhou, W. Xiong, L. J. Jiang, M. Mahjouri-Samani, P. Thirugnanam, X. Huang, M. M. Wang, L. Jiang and Y. F. Lu, *APL Mater.*, 2013, **1**.
- 15 P. Xu, J. Kang, J. B. Choi, J. Suhr, J. Yu, F. Li, J. H. Byun, B. S. Kim and T. W. Chou, *ACS Nano*, 2014, **8**, 9437–9445.
- 16 I. Popoola, M. Gondal, L. Oloore, A. J. Popoola and J. AlGhamdi, *Electrochim. Acta*, 2020, **332**, 1–14.
- 17 K. Lee, H. Lee, Y. Shin, Y. Yoon, D. Kim and H. Lee, *Nano Energy*, 2016, **26**, 746–754.
- 18 F. Thissandier, A. Le Comte, O. Crosnier, P. Gentile, G. Bidan, E. Hadji, T. Brousse and S. Sadki, *Electrochem. commun.*, 2012, **25**, 109–111.
- 19 H. Ghannam, J. P. B. Silva and A. Chahboun, *RSC Adv.*, 2021, **11**, 23346–23354.
- 20 H. Ji, X. Zhao, Z. Qiao, J. Jung, Y. Zhu, Y. Lu, L. L. Zhang, A. H. MacDonald and R. S. Ruoff, *Nat. Commun.*, 2014, **5**.